The random co-polymer glatiramer acetate rapidly kills primary human leukocytes through sialic-acid-dependent cell membrane damage

Christiansen, Stig Hill; Zhang, Xianwei; Juul-Madsen, Kristian; Hvam, Michael Lykke; Vad, Brian Stougaard; Behrens, Manja Annette; Thygesen, Ida Lysgaard; Jalilian, Babak; Pedersen, Jan Skov; Howard, Ken; Otzen, Daniel; Vorup-Jensen, Thomas

Published in:
Biochimica et Biophysica Acta. Biomembranes

Link to article, DOI:
10.1016/j.bbamem.2017.01.001

Publication date:
2017

Document Version
Peer-review version

The random co-polymer glatiramer acetate rapidly kills primary human leukocytes through sialic-acid-dependent cell membrane damage

Stig Hill Christiansen[a] [stig.hill@biomed.au.dk], Xianwei Zhang[a] [xianwei.zhang@biomed.au.dk], Kristian Juul-Madsen[a] [juul-madsen@biomed.au.dk], Michael Lykke Hvam[b] [mhvam@inano.au.dk] Brian Stougaard Vad[b] [bsv@chem.au.dk], Manja Annette Behrens[b] [mab@inano.au.dk], Ida Lysgaard Thygesen[b,c] [idathyge@gmail.com], Babak Jalilian[a] [jalilian.b@gmail.com], Jan Skov Pedersen[b] [jsp@chem.au.dk], Kenneth A. Howard[b,d] [kenh@inano.au.dk], Daniel E. Otzen[b] [dao@inano.au.dk], and Thomas Vorup-Jensen[a,b,d,e,f] [vorup-jensen@biomed.au.dk]

[a]Dept. of Biomedicine, Aarhus University, The Bartholin Building (1240), Bartholins Allé 6, DK-8000 Aarhus C, Denmark. [b]Interdisciplinary Nanoscience Center (iNANO), Aarhus University, Gustav Wieds Vej 14, DK-8000 Aarhus C, Denmark. [c]Dept. of Micro- and Nanotechnology, Technical University of Denmark, Ørsteds Plads. Building 345C, DK-2800 Kgs. Lyngby, Denmark. [d]The Lundbeck Foundation Nanomedicine Center for Individualized Management of Tissue Damage and Regeneration (LUNA) Aarhus University. [e]MEMBRANES Research Center, Aarhus University. [f]Center for Neurodegenerative Inflammation Prevention (NEURODIN), Aarhus University.

Corresponding author: Prof. Thomas Vorup-Jensen, MSc PhD DMSc. Biophysical Immunology Laboratory, Dept. of Biomedicine, Aarhus University, The Bartholin Building (1240), Bartholins Allé 6, DK-8000 Aarhus C, Denmark, phone (+45) 8716 7853; fax (+45) 8619 6128; e-mail vorup-jensen@biomed.au.dk

Abstract

The formulation glatiramer acetate (GA) is widely used in therapy of multiple sclerosis. GA consists of random copolymers of four amino acids, in ratios that produce a predominantly positive charge and an amphipathic character. With the extraordinary complexity of the drug, several pharmacological modes-of-action were suggested, but so far none, which rationalizes the cationicity and amphipathicity as part of the mode-of-action. Here, we report that GA rapidly kills primary human T lymphocytes and, less actively, monocytes. LL-37 is a cleavage product of human cathelicidin with important roles in innate immunity. It shares the positive charge and amphipathic character of GA, and, as shown here, also the ability to kill human leukocyte. The cytotoxicity of both compounds depends on sialic acid in the cell membrane. The killing was associated with the generation of CD45+ debris, derived from cell membrane deformation. Nanoparticle tracking analysis confirmed the formation of such debris, even at low GA concentrations. Electric cell-substrate impedance sensing measurements also recorded stable alterations in T lymphocytes following such treatment. LL-37 forms oligomers through weak hydrophobic contacts, which is critical for the lytic properties. In our study, SAXS showed that GA also forms this type of contacts. Taken together, our study offers new insight on the immunomodulatory mode-of-action of positively charged co-polymers. The comparison of LL-37 and GA highlights a consistent requirement of certain oligomeric and chemical properties to support cytotoxic effects of cationic polymers targeting human leukocytes.

Key words: cationic co-polymers, glatiramoids, immunotherapy, cathelicidins.

Introduction

Polymer-based formulations are currently among the most widely sold drugs (1). One of these is Copaxone™ with the pharmaceutical active ingredient glatiramer acetate (GA), approved for treatment of relapsing-remitting multiple sclerosis (MS). Both experimental and clinical studies suggest that GA has a broad impact on the immune system. Unlike other immunomodulatory MS drugs, GA has few side effects and does not increase the incidence of infections in treated patients. Among several proposals, the pharmacological mode-of-action appears to involve attenuation of the autoimmune response in MS by skewing of the T lymphocyte response from a Th1 to Th2 profile. More recently, cellular compartments and molecular mechanisms of the innate immune response has also been considered as targets for GA (2-5).

GA is prepared from random co-polymerization of *N*-carboxy-α-amino acid anhydrides using well-established polymerization techniques. The copolymers are composed of four amino acids, *i.e.*, L-glutamate, L-lysine, L-alanine, and L-tyrosine in molar ratios of 1.4 (Glu): 3.4 (Ala): 4.2 (Lys): 1 (Tyr) (2). The M_r varies from 5,000-9,000, corresponding to ~45-80 residues with an experimentally mean M_r of 8,030 and a narrow standard deviation of only 170 (6). Considering these properties, treatment with GA theoretically could generate more than 10^{30} different amino acid sequences (2,7). At physiological pH, the amphipathic co-polymers would carry an average net charge of ~+3 as judged from the molar ratios of glutamate and lysine. Synchrotron radiation circular dichroism (CD) suggests that the copolymers are largely disordered in aqueous solution, while membrane-like environments induce a high level of α-helical structure (8). Recently, it was appreciated that GA belongs to the realm of first-generation nanomedicines from the observation that co-polymers appear to form oligomers in solution (9 ,10). However, structural and functional characteristics of GA are poorly understood, in particular with regard to

what forces drive such oligomerization and the significance of this observation in terms of GA pharmacology.

GA treatment involves daily, subcutaneous injections of 18 mg GA or, more recently, 36 mg GA three times a week. Following subcutaneous injection, a substantial fraction of the GA dose is hydrolyzed (11), while the remaining GA copolymers interacts with peripheral blood lymphocytes locally in the skin(7). Koenig *et al.* (12) reported that GA co-polymers binds onto human cell lines, apparently through electrostatic contacts with heparan sulfate (HS) as well as proteins carrying negatively charged carbohydrates expressed in the cell membrane. It was already known that lysine residues are critical for GA prevention in experimental autoimmune encephalomyelitis (EAE)(13), an animal model for multiple sclerosis. The simpler poly L-lysine can also prevent EAE in guinea pigs (14). Hence, the positively charged residues of GA may play an important role in its pharmacological mode-of-action, but insight on mechanisms relating the requirement of positive charge to its immunomodulatory effects are lacking.

The cationicity and amphipathicity of GA are strikingly similar to the positively charged antimicrobial peptide (AMP) LL-37, which is the only human cathelicidin among a family of proteins widely found in mammals (15). AMPs were originally described on the basis of their striking ability to destroy the integrity of microbial membranes. Similar to GA (8), LL-37 also takes a mainly helical secondary structure in lipid membranes or membrane-like environments (16). It is now clear that functions of AMPs expand into several immunomodulatory properties (15,17-19). In psoriatic lesions, concentrations of LL-37 may reach ~6 mg/ml (20). Intriguingly, this is close to the concentration of GA co-polymers injected into the subcutaneous tissue of MS patients. LL-37 has long been known to kill leukocyte cell lines (21). While the general chemical nature of GA and its similarity with LL-37 does not, *per se*, dictate similar functions, no previous report has experimentally compared GA with such immunomodulatory peptides of the innate immune system.

Here, we report that GA kills primary human PBMCs, notably T lymphocytes, but also, albeit to a lesser extent, monocytes, at therapeutically relevant dosages. This occurred in the presence of albumin, physiological salt concentration, and divalent cations. Decoration with sialic acid was critical for such lysis. Both in qualitative and quantitative terms, LL-37 had similar effects. Imaging flow cytometry of cells treated with fluorescently-tagged GA found the compound to bind T lymphocytes extensively with indications of concomitant cell membrane deformation. LL-37 fragmented leukocytes into pieces easily quantitated by the forward scatter in flow cytometry. By contrast, the fragments generated by GA were smaller, in a size range of 180-500 nm as investigated by nanoparticle tracking analysis (NTA). GA was also capable of lysing liposomes with a zwitterionic composition similar to mammalian cell membranes. GA or LL-37 reduced the ability of T lymphocytes to form contact with the substrate, agreeing well with the notion that these compounds influences properties of the cell membranes. Taken together, our report now points to GA as a potential limiter of T lymphocyte functions. Surprisingly, the comparison with LL-37 reveals new aspects of the immunomodulatory effects of both compounds, notably with GA potentially mimicking functions of the evolutionary highly conserved LL-37.

Materials & Methods

Blood collection.

PBMC were isolated from buffy coats from The Blood Bank, Dept. of Clinical Immunology, Aarhus University Hospital made available through ethically approved procedures.

T lymphocyte and monocyte viability following GA and LL-37 exposure

Buffy coats were depleted of erythrocytes by Ficoll-Paque PLUS gradient centrifugation (GE Health Care Bioscience AB, Sweden). Immediately afterwards, T lymphocytes and monocytes, respectively, were isolated using Dynabeads® Untouched™ Cell Isolation kits according to manufacturer's instructions (Thermo Fisher Scientific, Waltham, MA). T lymphocytes and monocytes were either left untreated or stimulated for 30 minutes with GA (PubChem CID: 3081884; Copaxone®, Teva Pharmaceutical Industries Ltd, Petah Tikva, Israel; Batches X07861 & P63010) or LL-37 (PubChem CID: 16198951), made by Innovagen, Lund, Sweden as described (22), at concentrations of 2, 10, 25, or 50 μg/ml in temperate serum-free Gibco® AIM-V medium (Thermo Fisher Scientific) supplemented with 1 % (w/v) GlutaMax (Thermo Fisher Scientific) and 10 mM HEPES (Thermo Fisher Scientific). All indicated concentrations were calculated from dilutions of the Copaxone stock at 20 mg/ml GA. Cells were centrifuged at 230×*g* for 7 min at room temperature. Cells were resuspended in 500 μl PBS. Staining with mAb was conducted at room temperature for 20 min by addition of 10 μl of anti CD45-FITC (DAKO A/S, Copenhagen, Denmark), 3 μl of CD3-PE (DAKO), 10 μl of CD19-FITC (DAKO), and 10 μl of anti CD14-APC (BD Biosciences, Franklin Lakes, NJ). To quantify viability, cells were stained with 10 μl of 7-amino-actinomycin D (7AAD, BD Biosciences). All samples were stained for 20 min at room temperature in complete darkness. Then, cells were washed twice with 2 ml PBS supplemented with 0.5% (w/v) BSA and 0.09% (w/v) NaN_3 and centrifuged at 230×g for 7 min and finally resuspended

in 200 µl supplemented PBS. To quantify the absolute count of cells in samples, fluorescent counting beads, with laser excitation at 488 nm and light emission at 530-700 nm, were applied according to manufacturer's protocol (Cytocount™, DAKO). In these experiments, all flow cytometry data were collected on a LSRFortessa (BD Biosciences) instrument and analyzed using FlowJo V.10.0.8 software (FlowJo, Inc., Ashland, OR).

Quantification of cell death induced by GA and LL-37 in physiological media

Prior to analysis, PBMCs from three separate donors were stored at -134°C in round-bottom cryo tubes (Nunc®, Thermo Scientific) in RPMI 1640 with L-glutamine, pH 7.2, 20% (v/v) heat-inactivated fetal calf serum (FCS; Gibco®, Thermo Fisher Scientific), and 10% (v/v) DMSO. Cells were thawed quickly at 37°C, transferred to 15 ml tubes with 9 ml PBS, pH 7.4, and 20% (v/v) FCS, and centrifuged for 10 min at 200×*g* at 20°C with slow braking. Supernatants were discarded and cells resuspended in HEPES-Buffered Saline (HBS) (pH 7.4, NaCl 0.15 M, KCl 5 mM, $MgCl_2$ 1 mM, $CaCl_2$ 1.8 mM; HEPES 10 mM) or HBS (pH 7.4, NaCl 0.15 M, KCl 5 mM, $MgCl_2$ 1 mM, $CaCl_2$ 1.8 mM; HEPES 10 mM) supplemented with 40 mg/ml of human serum albumin, close to the concentration in human plasma (23), to a final concentration of 1×10^6 cells/ml. PBMCs were either left untreated or stimulated for 60 minutes with GA or LL-37 at concentrations of 2, 10, 25, or 50 µg/ml. Then, cells were washed once with PBS, stained with 7AAD and prepared for flow cytometry following procedures as previously described.

Leukocyte viability following neuraminidase treatment and GA and LL-37 exposure

Freshly isolated PMNCs were prepared from buffy coats as above. Immediately after isolation, the MNCs were either left untreated or incubated with 50 mU/ml neuraminidase obtained from *Vibrio cholerae* (50 mU/ml; Cat.no: 72197-1ML, Sigma-Aldrich, St. Louis, MO) at 37°C for 30 min.

Subsequently, cells were left untreated or treated with 50 µg/ml GA (Teva) or LL-37 (Innovagen) for 30 min at 37°C as described above. Staining with mAb was conducted in complete darkness at room temperature for 20 minutes by addition of 5 µl CD45-FITC+CD14-RPE (FR700, DAKO), 3 µl of CD3-PE (R0810, DAKO, 10 µl of CD14-PE (345785, BD Bioscience), and 5 µl of CD45-FITC (F0861, DAKO). To quantify viability, cells were stained with 10 µl of 7AAD. Then, cells were washed twice with 2 ml PBS supplemented with 0.5% (w/v) BSA and 0.09% (w/v) NaN_3 and centrifuged at 230×*g* for 7 min. Finally, cells were resuspended in 150 µl PBS supplemented with 0.5% (w/v) BSA and 0.09% (w/v) NaN_3. Flow cytometry data were collected on a Novocyte™ (ACEA Biosciences Inc., San Diego, CA) and analyzed using FlowJo.

Visualization of fluorescently tagged GA on leukocytes by imaging flow cytometry

GA was labeled with Pacific Blue (Molecular Probes®, Thermo Fisher Scientific) according to manufacturer's instructions. PBMCs from two donors were thawed and prepared as described above. The cells were resuspended in PBS to a final concentration of 2×10^6 cells/ml and either left untreated or treated with 20 µg/ml labeled GA for 30 minutes under conditions as described above and resuspended in 1 ml PBS. Staining with monoclonal antibodies was conducted at room temperature for 15 min by addition of 20 µl CD3-PE (DAKO), 20 µl CD14-APC (BD) and CD45-FITC (DAKO). To quantify viability, cells were stained with 20 µl of 7AAD, washed twice in 1 ml PBS, and centrifuged at 230×*g* for 7 min. Finally, cells were resuspended in 50 µl PBS. Flow cytometry was made with the Amnis ImageStream^X MKII instrument, using an objective with 60-times magnification, and analyzed with the IDEAS® software package (Amnis Corporation, Seattle, WA). Cell membrane circularity (ζ) was calculated from the average distance of the object boundary from its center ($\overline{R_i}$) divided by the variation of this distance:

(Equation 1) $$\zeta = \frac{\overline{R_i}}{VAR(\overline{R_i})}$$ (24).

Nanoparticle tracking analysis of leukocyte debris

Prior to analysis, PBMCs from three separate donors were stored at -134° C in round-bottom cryo tubes (Nunc®, Thermo Scientific) in RPMI 1640 with L-glutamine, pH 7.2, 20% (v/v) heat-inactivated fetal calf serum (FCS; Gibco®, Thermo Fisher Scientific), and 10% (v/v) DMSO. Cells were thawed quickly at 37°C, transferred to 15 ml tubes with 9 ml PBS, pH 7.4, and 20% (v/v) FCS, and centrifuged for 10 min at 200×*g* at 20° C with slow braking. Supernatants were discarded and cells resuspended in PBS, pH 7.4 to a final concentration of 1×10^5 cells/ml. One ml of cell suspension was aliquoted into 1.5 ml tubes. The cells were then treated with GA (Teva) or LL-37 (Innovagen) in concentrations of 0.2, 1.0, 5.0, or 10 µg/ml by incubation in a rotator mixer at 10 rpm shaking 4 times in each half rotation for 30 min at 37°C. Next, to remove intact cells from the suspension, the cell suspensions were centrifuged at 2,000×*g* for 10 min, followed by transfer of 700 µl of the supernatant to new 1.5 ml tubes while carefully avoiding the pellet. Samples were submitted to analysis within less than three hours. Particles present in the sample were analyzed using the NanoSight LM10 system (Malvern Instruments Ltd., Malvern, UK). The system was configured with a 405-nm laser and a high sensitivity sCMOS camera (OrcaFlash2.8, Hamamatsu C11440, Malvern). Videos were recorded and analyzed using the NTA software (version 2.3 build 0025). The minimum track length, blur, and expected particle size were all set to automatic. The room temperature during measurements was recorded manually and ranged from 23°C to 25°C. All samples were thoroughly mixed before measurements, which were initialized within 10 s of injection into the measurement chamber. Approximately 30-50 particles were in the field of view and concentration of particles in samples ranged from 2×10^8-1.2×10^9 particles/ml. Typically, the number of completed tracks for each measurement exceeded 2000. For the untreated samples as

well as for each concentration of either GA or LL-37, three videos of 60 s were recorded. From these replicates, an average histogram was calculated. Finally, the mean distribution was calculated from the average histograms obtained in experiments with cells from three donors.

GA-induced lysis of lipid vesicles and structural response to contact with liposome

Phospholipids used were 1,2-dioleoyl-sn-glycero-3-phosphocholine (DOPC) or 1,2-dioleoyl-sn-glycero-3-phospho-rac-(1-glycerol) (DOPG), both from Avanti Polar Lipids (Alabaster, AL). Large unilamellar vesicles (LUV) containing calcein were prepared by vortexing a phospholipid suspension in 20 mM Tris HCl, pH 7.5, containing 70 mM calcein sodium salt, to a final concentration of 10 g/l phospholipid (~14 mM). The LUVs were exposed to at least seven cycles of freezing in liquid nitrogen, followed by thawing in a 50°C water bath and extrusion through a 200 nm-pore filter 12 times using a 10 ml thermo barrel extruder (Northern Lipids, Vancouver, Canada). The lipid suspensions were run on a PD10 column (GE Healthcare), pre-equilibrated with 20 mM Tris HCl, pH 7.5. The release of free calcein from the vesicles and the subsequent increase in fluorescence were monitored by excitation at 490 nm, recording emission at 515 nm every second using a slit-width of 2.5 nm in a Cary Eclipse Fluorescence spectrofluorimeter (Varian, Palo Alto, CA). The vesicles were diluted to a concentration of ~0.017 g/l (20 μM). GA was applied to experiment either as the raw drug formulation or following dialysis in Slide-A-Lyzer® 10K Mini (Thermo Scientific) against isotonic buffer (150 mM NaCl, 5 mM KCl, 1 mM $MgCl_2$, 1.8 mM $CaCl_2$, pH 7.4). Initially, samples were dialyzed in a volume of 0.5 l per 100 μl of GA (20 mg/ml) for 1h, followed by the change of buffer and a second dialysis step for 2 h. The dialysis buffer was changed again and the samples left o/n. All steps were performed at 20°C. GA passing through the dialysis membrane in the first dialysis step was also applied to the experiments. GA concentrations were calculated using an Abs 0.1 % (= 1g/l·cm) of 1.519 at 280 nm. Following injection of GA, the

dye signal at the emission wavelength was followed until it reached a plateau, typically after 35 minutes.

The structural consequences of the contact between the GA polymers and the liposomes were investigated by circular dichroism spectroscopy (CD) essentially as described earlier (25). The spectra were collected in 1-mm path length quartz cuvettes on a Jasco J-810 spectropolarimeter with a model No. PTC-348W1 temperature control unit (Jasco, Spectroscopic Co., Hachioji, Japan). Spectral scans were performed from 250 to 195 nm, with a step resolution of 0.1 nm and bandwidth of 1.0 nm at 50 nm/min averaged over five repeats at 20°C under a nitrogen atmosphere. The GA concentration was set at 0.2 mg/ml. Lipids were titrated into the cuvette and allowed to equilibrate for 2 min before measurement.

Small-angle X-ray scattering measurements and data analysis

Small-angle X-ray scattering (SAXS) measurements data on GA was collected on the in-house NanoStar camera in the Dept. of Chemistry, Aarhus University, optimized for solution scattering (26). Following dialysis in Slide-A-Lyzer® 10K Mini (Thermo Fisher Scientific) units for 24 h with two changes of buffer, either with isotonic HEPES buffer as above or 10 mM HEPES, pH 7.4 buffer, the GA concentration was adjusted to 1.3, 2.6, or 5.3 mg/ml, respectively, with dialysis buffer. Concentrations were calculated from the light absorption at 280 nm as described above. The samples were kept at 25°C in home-built re-usable quarts capillaries during the measurements. From measurements on the corresponding buffers in the same capillary, the data on GA were background subtracted and converted to absolute scale using water as a primary standard with the SUPERSAXS program package (J.S.P, unpublished). Finally the intensity, *I(q)*, is displayed as a function of the scattering vector, q, defined as $q = 4\pi \cdot \sin(\theta)/\lambda$, where λ is the X-ray wavelength at 1.54 Å and 2θ is the scattering angle between the incident and scattered beam.

The molecular mass and overall size of the particles was determined using an indirect Fourier transformation analysis (IFT) (27,28). The IFT data from analysis provides information on the radius of gyration R_g and weight-average molecular mass as well as in the form of the molecules. The results and the q dependence of the measured data suggested that the polypeptides are present as linear structures with some flexibility. Therefore, a model of semi-flexible, self-avoiding polymer chains with a finite cross section was applied to the data (29). The model contains three parameters, the contour length of the chains L^h, the Kuhn length, equal to twice the persistence length, which described the flexibility of the chains and the cross-section radius R of the chains.

The conformations of the polypeptides were further investigated by applying the ensemble optimization method (EOM) (30) In this method, a large pool of structures is generated, followed by a generic algorithm selection of the subset of structures best fitting the experimental data to represent the solution conformation of GA.

Electric cell-substrate impedance sensing assay

The electric cell-substrate impedance sensing (ECIS) assay was modified from the manufacturer's instruction. T lymphocytes were isolated as described above. Freshly isolated T-cells were suspended to a concentration of 3×10^6 cells/ml in 150 mM NaCl, 5 mM KCl, 1 mM $MgCl_2$, 1.8 mM $CaCl_2$, 10 mM HEPES, pH 7.4, supplemented with 0.1 mg/ml HSA and 5 mM D-glucose. Stock solutions of either LL-37 or GA were made in PBS, pH 7.4, at concentrations in 200-fold excess. A volume of 2.5 µl of stock solution, or pure PBS as a control, was added to 0.5 ml of cell suspensions followed by careful mixing. The mixtures were transferred to E-plate L8 (ACEA) and installed in iCELLigence equipment (ACEA) for recording the changes in impedance over 8 h with incubation at 37°C and 5 % (v/v) CO_2. Experiments were repeated three times with cells from different donors.

Results

GA and LL-37-mediated leukotoxicity

We compared the influences of LL-37 with GA on purified primary T lymphocytes and monocytes. As noted above, the glatiramer co-polymers and LL-37 share their cationic and amphipathic properties. Accordingly, it seemed appropriate to test both compounds for one of the known influences of LL-37 on cells, namely its cell toxicity (31-34). As a starting point, we chose concentrations of GA and LL-37 of 2-50 μg/ml, similar to the range used by Koenig *et al.* for GA stimulation of cytokine production by RAW264.7 and murine bone-marrow-derived dendritic cells (12). To distinguish leukocytes population, fluorophore-conjugated antibodies to CD3 (a marker for T lymphocytes), CD14 (a marker for monocytes), and CD45 (broadly expressed on all leukocytes) were used.

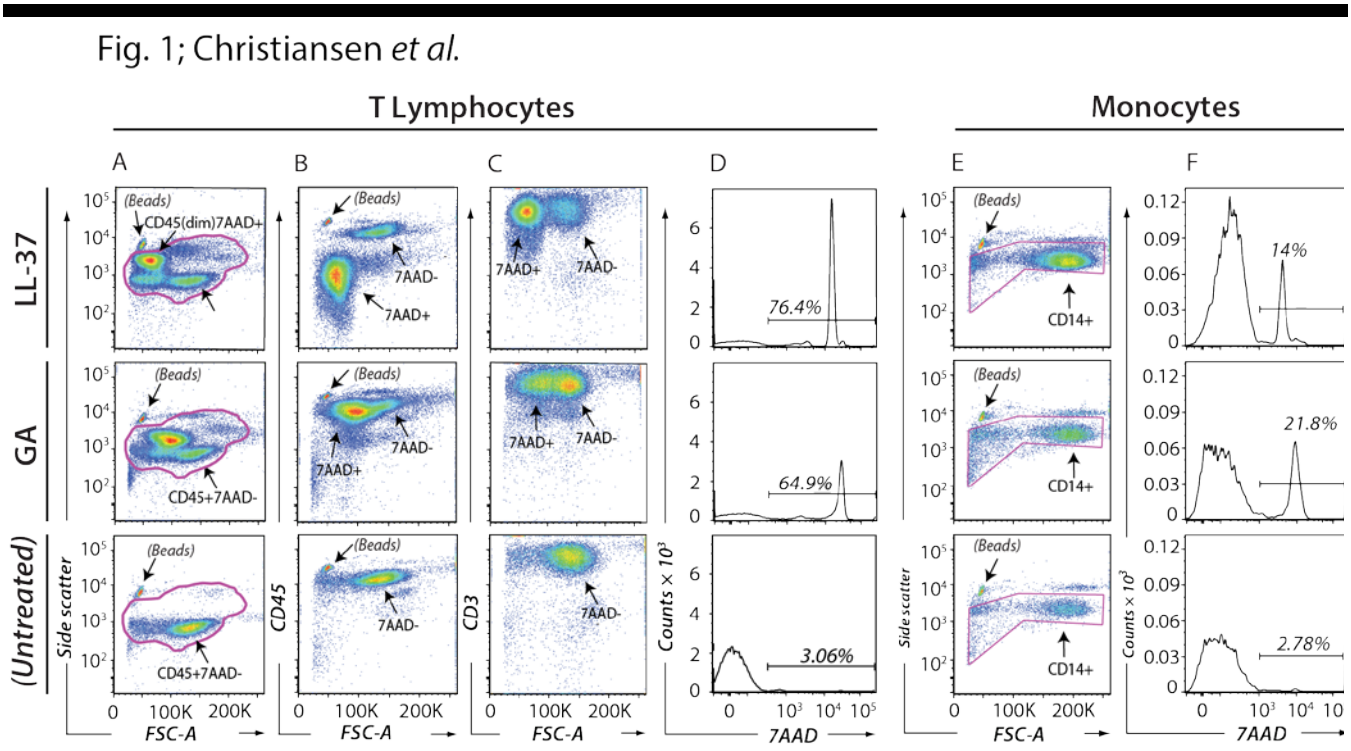

T lymphocyte and monocyte viability following incubation with GA or LL-37. *A-E*, Purified T lymphocytes in the presence of fluorescent beads counting were either left as untreated or treated with 50 µg/ml LL-37 or GA. Following 30 min of incubation, cells were stained with antibodies to CD3 and CD45 as well as 7AAD. For comparison of size-alterations in the treated and untreated cells, the cellular distribution was compared in Forward/Side scatter plots (*A*) as well as the distribution in CD45/Forward scatter (*B*) and CD3/Forward scatter plots (*C*). The staining with 7AAD was presented as histograms with an indication of the percentage of stain-positive cells among the un-gated cells. *E-F*, Purified monocyte viability following incubation with 50 µg/ml GA or LL-37 or without treatment. For comparison of size-alterations, the cellular distribution was compared in Forward/Side scatter plots (*E*). The 7AAD stain-positive cells among the un-gated cells were analyzed in a histogram (*F*).

To ensure direct comparability between samples, counting beads were included to fix the number of events analyzed. In T lymphocytes, after 30 min of incubation both LL-37 and GA generated at least two populations of events positive for 7AAD with low forward scatter and separated by their side scatter (Fig. 1A). For both compounds, an easily identifiable population of $CD45^{dim}$ events emerged after LL-37 treatment, while GA treatment caused a similar, but less, reduction in the CD45 staining (Fig. 1B). The reduction in forward scatter did not accompany a loss in CD3 expression for any of the treatments (Fig. 1C). Both LL-37 and GA treatment led to a large increase

Fig. 2; Christiansen *et al.*

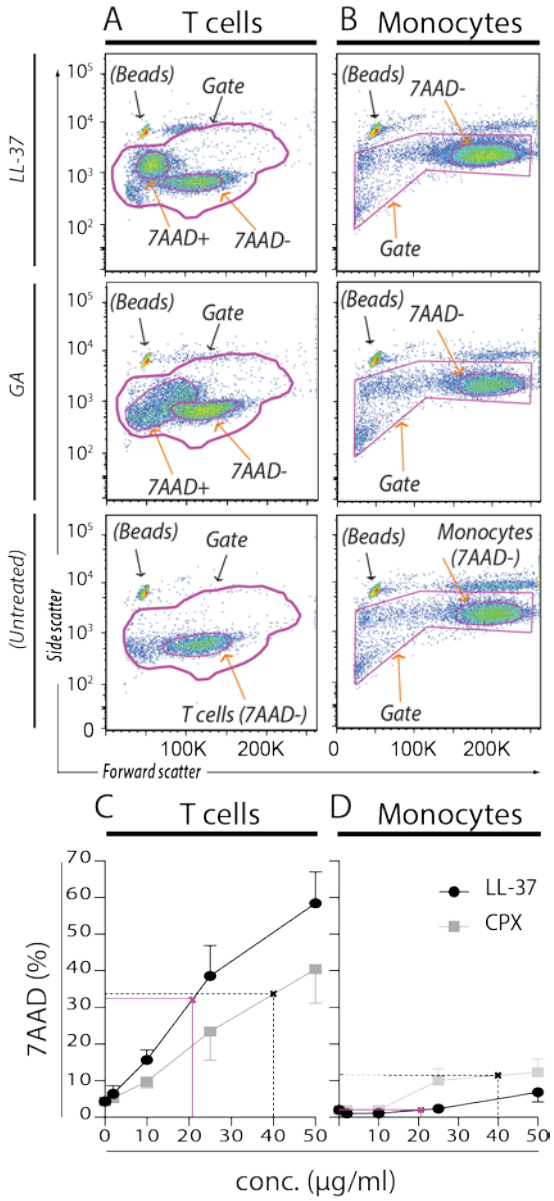

Quantification of cell death induced by GA and LL-37 in purified T lymphocyte and monocyte populations. *A*, Gating of T lymphocytes. Compared with untreated cells, a population of 7AAD$^+$ cells was discernible based on a lower forward scatter following treatment with GA or LL-37. The percentage of 7AAD$^+$ and live (7AAD$^-$) T lymphocytes is indicated in the Forward/Side scatter plots. A gate was placed covering both populations ("Gate") and excluding counting beads. *B*, Gating of monocytes. Since monocytes were only moderately affected by GA and LL37, a broad gate ("Gate") covering all CD14$^+$ cells, but excluding counting beads, was placed to capture change in the 7AAD staining. *C-D*, Based on the gates shown in Panels A & B, enumeration of the percentage of 7AAD positive T lymphocytes (*C*) or monocytes (*D*) following no treatment or treatment with 2, 10, 25, or 50 µg/ml of LL-37 or GA. The plots indicate the mean value ± SEM from separate experiments made with cells from five BD. The solid pink line and the dashed black line indicates the activity of, respectively, LL-37 and GA at equimolar concentrations (5 µM).

in the 7AAD staining (Fig. 1D). In purified monocytes, the response was qualitatively and

quantitatively different, with a moderate, but detectable, change in the forward or side scatter following LL-37 and GA treatment (1F). The 7AAD staining increased when treating the monocytes with GA, while LL-37 had only a minor effect (Fig. 1G).

To capture all dead T lymphocytes (Fig. 2A) and monocytes (Fig. 2B), we devised a gating strategy, which ensured inclusion of all dead cells or debris generated by the treatments. The induced effects were quantitatively consistent for the five donors analyzed (Fig. 2 C, D). In the analysis of T lymphocytes mixed with 50 µg/ml GA, ~40% of the events were positive for 7AAD. The response was titratable down to ~2-10 µg/ml (Fig. 2C). In the case of LL-37, the results were similar although slightly increased compared with GA (Fig. 2C). When incubating monocytes with LL-37 or GA, GA produced stronger 7AAD staining at 12% than LL-37, which only reached 7%, with both compounds used at 50 µg/ml. At equimolar concentrations (5 µM) LL-37 and GA were equally effective at killing T lymphocytes, while GA achieved higher killing efficiency in monocytes than LL-37.

GA retains its lytic capabilities in media with high divalent cation and protein concentration

Several studies addressed the activity of AMPs, including LL-37, in high salt concentrations and under serum-like conditions, and reported their activity to be reduced(35). Hence, we tested the killing activity of GA and LL-37 on MNCs resuspended in media with a physiological salt concentration and composition, further supplemented with 40 mg/ml HSA (Fig 3). We found that both GA and LL-37 maintained their activity in a HBS buffer with Mg^{2+} and Ca^{2} (Fig. 3B). The response was titratable down to ~2-10 µg/ml. Neither GA or LL-37 exhibited noticeably reduced the killing. In conclusion, both GA and LL-37 achieved similar killing capacities as observed in PBS. Conversely, the killing activity of LL-37 and GA were reduced to a similar level in the presence of serum concentrations of HSA at ~40 mg/ml (23). Surprisingly, the activity of LL-37

was, however, quenched at concentrations below 50 µg/mL, while the killing activity of GA was

Fig. 3; Christiansen *et al.*

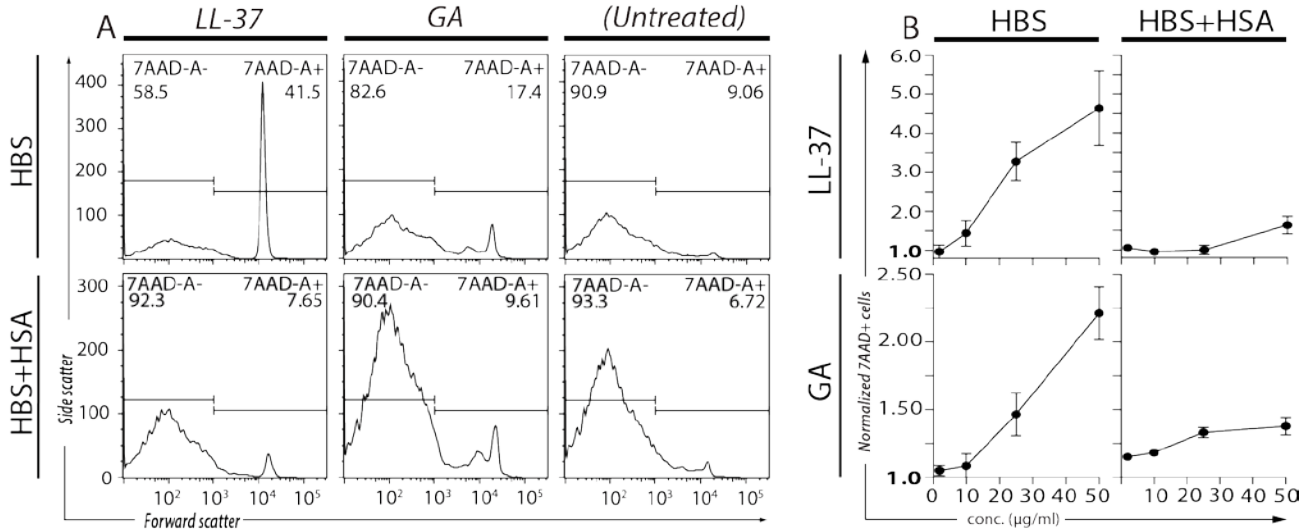

Quantification of cell death induced by GA and LL-37 in PBMCs resuspended in HEPES-buffered saline or HEPES-buffered saline supplemented with 40 mg/ml HSA to mimic human plasma. *A*, 7AAD stain-positive cells were analyzed in histograms following treatment with 25 µg/ml of LL-37 or GA. The number of 7AAD+ cells is indicated in percentage. *B*, Normalized 7AAD staining from experiments with four donors. The 7AAD staining was evaluated as described in Panel A. For each donor the normalized 7AAD staining was calculated from the staining treatment with 2, 10, 25, or 50 µg/ml of LL-37 or GA divided with the staining obtained for untreated cells. The plots indicate the mean value ± SEM.

titratable down to ~10-25 µg/mL.

GA and LL-37 lysis of T lymphocytes involves sialic acid

Based on the observations by Koenig *et al.* (12) on the role of heparan sulfate (HS)-carrying proteins in the binding of GA, we initially checked the expression of HS in primary PBMCs, including the T lymphocytes, according to previously established procedures (36). However, as also noted by others (36), resting leukocytes do not express HS quantitatively (data not shown). An alternative source of electrostatic interactions between the cationic polypeptides and cell membranes is sialic acid. The role of sialic acid in the cell killing by GA and LL-37 was analyzed

by treating PBMCs with neuraminidase (Fig. 4). The neuraminidase did not affect the light scattering properties (Fig. 4A), CD14 or CD45 expression (Fig. 4B), or viability of the MNC (Fig. 4C). As also shown in Fig. 2C-D, 10 µg/ml GA and LL-37 killed approximately 20% of the

Fig. 4; Christiansen *et al.*

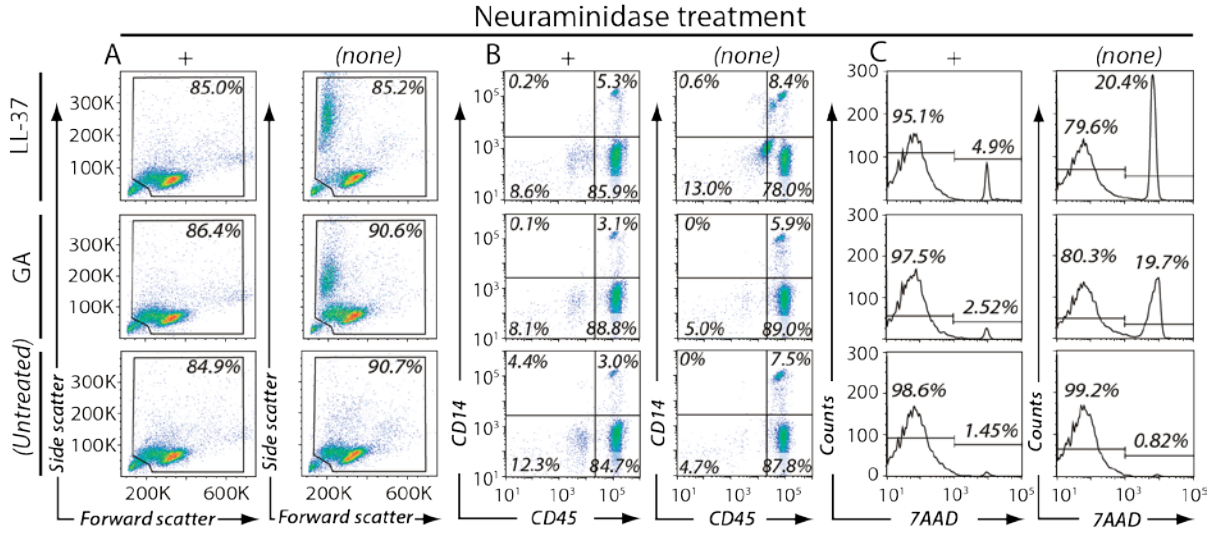

The influence of neuraminidase pre-treatment on GA or LL-37 killing of PBMCs. The cells were either pre-treated with neuraminidase (+) or left untreated (none), followed by exposure to GA, LL-37 or no treatment (untreated). The cells were analyzed according to their forward and side scatter distributions (*A*), the CD14 and CD45 expression (*B*) and 7AAD staining (*C*).

PBMCs.

In this experiment (Fig. 4), pre-treatment with neuraminidase lowered the killing by GA and LL-37 to 3% and 5%, respectively (Fig. 4C). These finding proved quite robust (Fig. 5). In PBMCs isolated from four donors, cells treated with neuraminidase in all cases proved less susceptible to killing by LL-37 (Fig. 5A) or GA (Fig. 5B), while the neuraminidase treatment itself did not alter the percentage of 7AAD-positive cells (Fig. 5C). The effect of neuraminidase treatment seemed most pronounced for LL-37, where the general trend was a two-fold reduction in killing as a

consequence of neuraminidase treatment (Fig. 5A). In the case of GA, at least for a single donor, the neuraminidase treatment reduced killing almost 9-fold by neuraminidase treatment while others showed a 1.5-2 fold reduction (Fig. 5B).

Fig. 5; Christiansen *et al.*

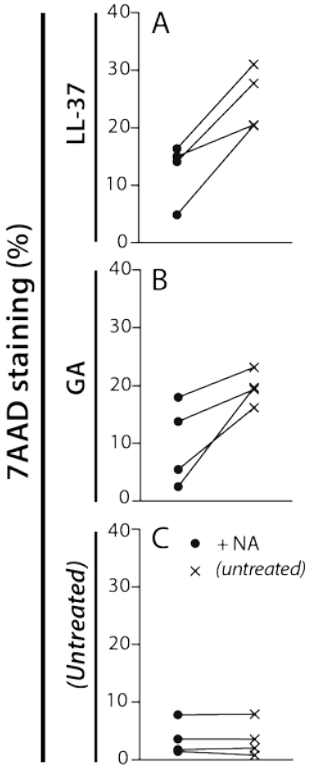

Quantification of the killing by GA (*A*) or LL-37 (*B*) of PBMCs from four donors with (•) or without (×) NA pretreatment. As a control, cells not receiving treatment with cationic molecules were analyzed (*C*). In all panels, experiments with cells from the same donor are indicated with connecting lines.

The binding of fluorophore-conjugated GA to T lymphocytes visualized by Imaging Flow Cytometry

PBMCs were characterized by Imaging Flow Cytometry with regard to the distribution of lymphocytes and monocytes (Fig 6A). From the observation made above on the high killing of T lymphocytes, these cells were further characterized based on their propensity to bind fluorophore-conjugated GA (GA^*) (Fig. 6A). In total, 30% of the CD3+ T lymphocytes stained positive for GA^*, whereas 37.1% CD3+ T lymphocytes remained GA^*-negative. Among the GA^*-positive T lymphocytes, a total of 78.9% stained positive for 7AAD, while only 0.89% of the GA^*-negative T lymphocytes were 7AAD positive as expected from the analyses mentioned above (Fig. 6B).

Next, we utilized the IDEAS® software package to quantify the circularity (ζ) of T lymphocytes. Based on CD45 fluorescent staining of viable T lymphocytes, this feature describes

the roundness of a T lymphocyte as quantified by Equation 1: the closer an object is to a perfect

Fig. 6; Christiansen *et al.*

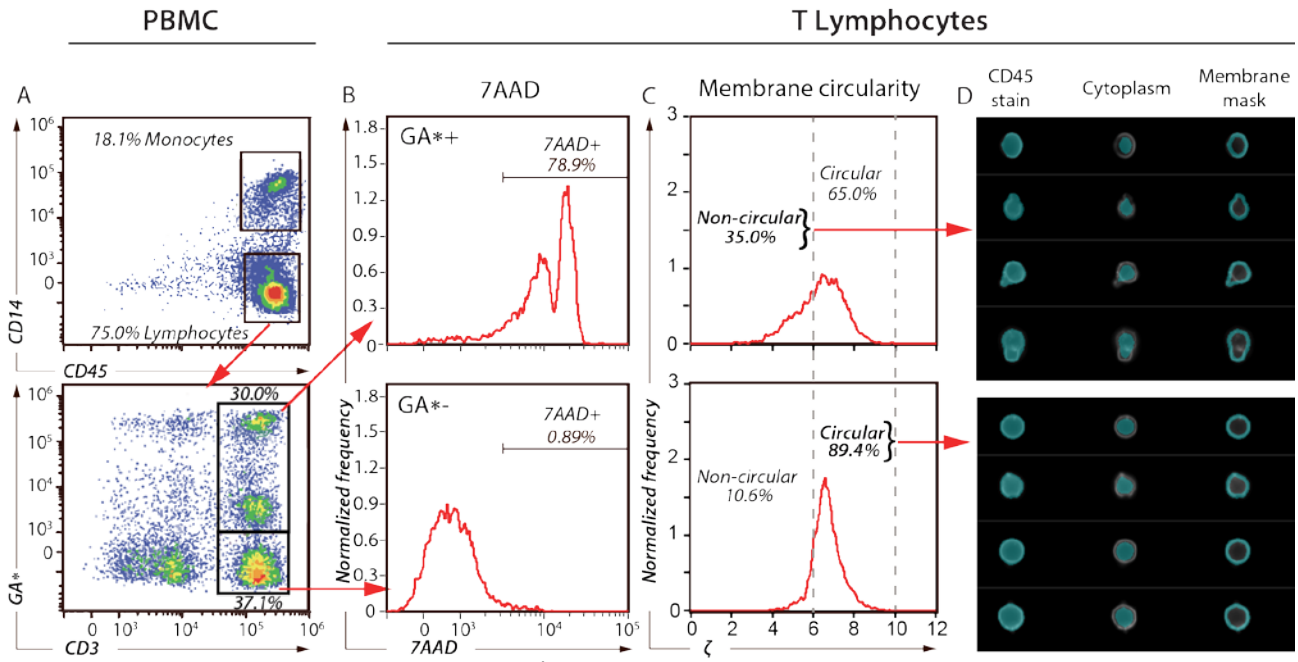

Visualization of fluorescently-tagged GA (GA*) binding to T lymphocytes using imaging flow cytometry. *A*, Following treatment with 20 µg/ml GA*, PBMCs were characterized based on their expression of CD14 and CD45 permitting gating of the T lymphocyte population based on the high expression of CD45 and low expression of CD14. Further gating was made by staining for CD3 and separating the T lymphocytes into one gate containing cell with high (30% of events) and low (37.1% of events) GA* staining. *B,C*, In the GA* high and low stain populations, the cells were analyzed for their 7AAD+ staining (B) and for cell membrane circularity (C) according to Equation 1. *D*, Morphology of circular and non circular cells depending on GA* staining. Four randomly chosen examples of non-circular cells (ζ<6) with GA* staining and circular cells (ζ>6) with low GA* staining. The cell membrane area was visualized using the CD45 staining. From the total stain CD45 ("CD45 stain"), the cytoplasmic region ("Cytoplasm") was identified by selecting the membrane perimeter as the five outermost stain-positive pixels (with a size of 300 nm × 300 nm). By subtracting the cytoplasmic part from the total stain, the membrane region was highlighted ("Membrane mask").

circle, the smaller the variation and, hence, the higher the circularity (24).

T lymphocytes staining positive for GA* had a relatively lower circularity as compared to T lymphocytes staining negative for GA*. Intriguingly, in T lymphocytes with lower circularity GA* was overlapping with the 7AAD staining, thereby indicating that GA* ultimately

penetrated T lymphocytes, even into the nuclear compartment (data not shown). A total of 87% of the monocytes stained positive for GA*, while 34% of those stained positive for 7AAD as expected from the experiments with unlabeled GA. Also in line with these experiments, monocytes were less affected by the treatment with GA*, and, in contrast to T lymphocytes, they retained a high circularity value despite the treatment with GA* (data not shown).

Fig. 7; Christiansen *et al.*

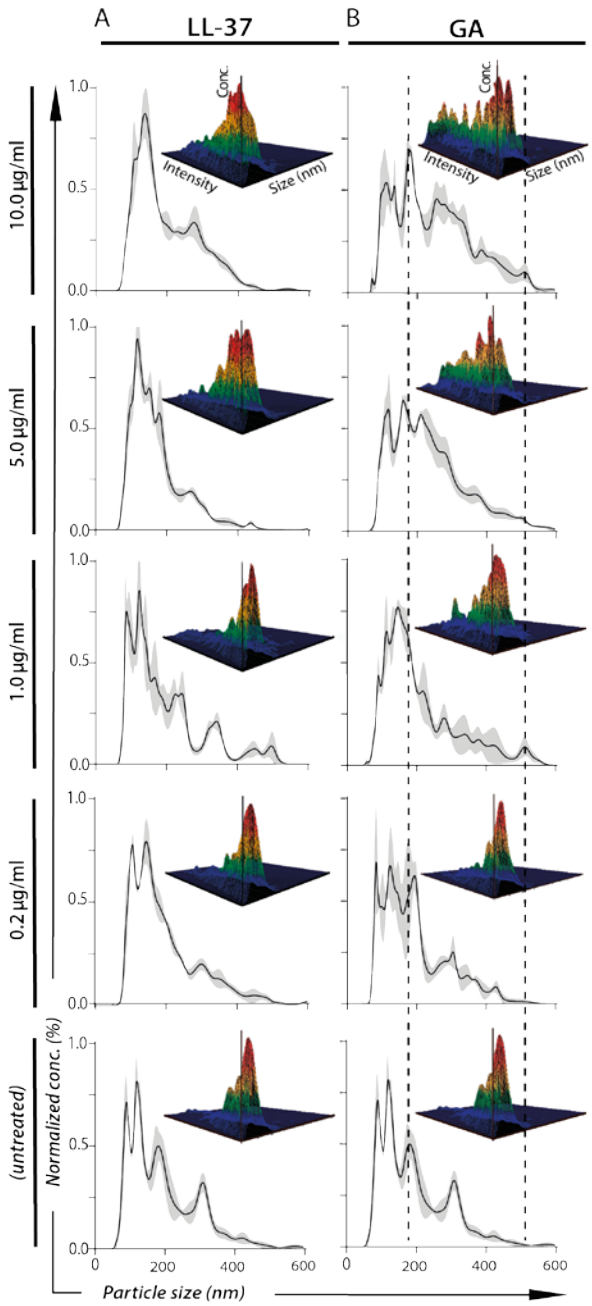

Fragmentation of PBMCs after treatment with LL-37 or GA followed by NTA. Following incubation of the PBMCs with LL-37 (*A*) or GA (*B*) at concentration ranging from 0.2-10 µg/ml, major debris was cleared by centrifugation as described in the Materials and Methods section and the supernatants subjected to NTA to characterize the size distribution (diameter) of the particles. To facilitate comparisons of the shifts in size distributions, the analysis of untreated cells are indicated below each set of treatment with either LL-37 or GA. The concentration of particles is presented as normalized to the total concentration of particles. All experiments were made with PBMCs from three donors with the mean concentration indicated with a solid, black line and the standard error of the mean for the measurements indicated in grey color. The raw data extracted from the NTA analysis is shown in inserts as the particle concentration plotted as a function of particle size and intensity of the scattered light. Hatched lines in *B* indicate the particle size interval from 180 to 500 nm.

Treatment of PBMCs with GA or LL-37 generates particles with different sizes

The analyses in Fig. 1, 2 and 4 clearly pointed to the formation of 7AAD+ particulate material as a consequence of leukocyte treatment with either GA or LL-37. We initially compared the change in forward scatter in the flow cytometer for treated cellular samples. Only at the relatively high concentration of 50 µg/ml GA or LL-37 (Fig. 1A), it was possible to follow such a size change in forward scatter. Inspection of diagrams clearly suggested that LL-37 was capable of forming particles with slightly lower forward scatter than GA. Lower concentrations than 50 µg/ml of LL-37 or GA did not generate any major detectable change in the forward scatter profile. However, low-forward scatter particles are only poorly resolved by standard flow cytometers. For this reason, we chose to analyze the low forward scatter particles with a recently developed methodology, in which nanoparticles are tracked through their scatter of a laser beam (Fig. 7). Separate experiments were carried out with PBMCs from three donors. The distribution of the particle sizes from the three donors is shown as the mean of the data indicated with a solid, black line. For each treatment in Fig. 7, a representative three-dimensional plot indicates the change in particle size, concentration and intensity of the scattered light upon treatment with either LL-37 (Fig. 7A) or GA (Fig. 7B). For treatments with GA, the size distribution altered in the direction of larger particles correlating with increasing GA concentrations. LL-37 also showed some change in size distribution. To better quantitate these changes, cumulative plots were made (Fig. 8). The size changes for LL-37 treatments were small and not correlated with the applied concentration. By contrast, in the case of GA, the median particle size, *i.e.*, the size separating the lower half from the higher half of the particles, changed from ~125 nm to ~175 nm in strict order with the applied concentration (Fig. 8B).

Fig. 8; Christiansen *et al.*

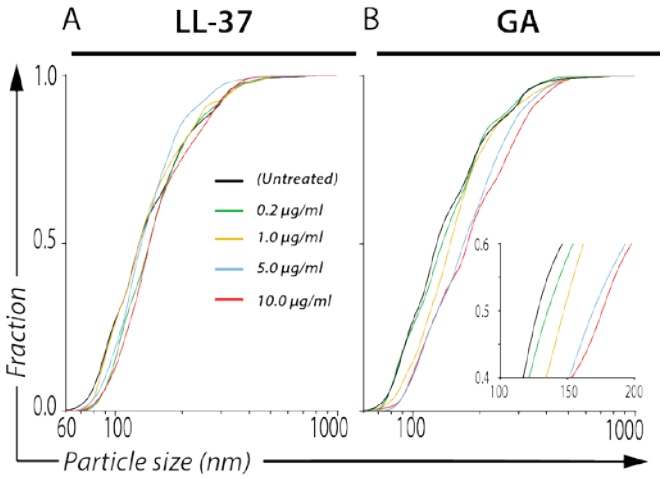

Cumulative particle size distributions calculated from the data presented in Fig. 7. The cumulative particle size distribution for PBMCs was calculated for treatments with 0.2-10 µg/ml LL-37 (*A*) or GA (*B*). For comparison, the cumulative plot for untreated cells is indicated in both panels. In Panel B, the insert magnifies the region of the median sizes in the interval ~125-150 nm.

Time-resolved measurements on the interaction between T lymphocytes and LL-37 and GA

Although the concentration of glatiramer acetate in blood cannot be determined directly, the bioavailability in some tissues or even in blood could be lower than the concentrations previously applied in this study. Hence, to study the effects of GA on T lymphocytes in low concentrations, we employed a time-resolved measurement of the interaction by the ECIS assay (Fig. 9). In this setting, the contact between the cells and the conducting substrate increases electrical resistance, here measured as the cell index. Apart from the addition of cationic polypeptides mentioned above, the cellular substrate contact is influence by a rapid, simple settling of the cells on the surface as well as a subsequent cellular reorganization to accommodate the surface contact.

T lymphocytes from a total three donors were analyzedfollowing the application of LL-37 in concentrations of 0.04-5 µg/ml (Fig. 9A) or GA in a concentration range of 0.2-5 µg/ml (Fig. 9B). Cells settled within ~20 min, followed by a slower rise in cell index, which plateaued in ~1 h. In all experiments, the cell index was lowered in a strictly concentration-dependent manner when applying either GA or LL-37. For both compounds, an influence down to a concentration of 1 µg/ml in all experiments could be observed. Lower concentrations did not change the cell index

reproducibly among the donors. The effect of the cationic polypeptides had a remarkably fast onset and persisted throughout the experiment for 2 hours.

Fig. 9; Christiansen *et al.*

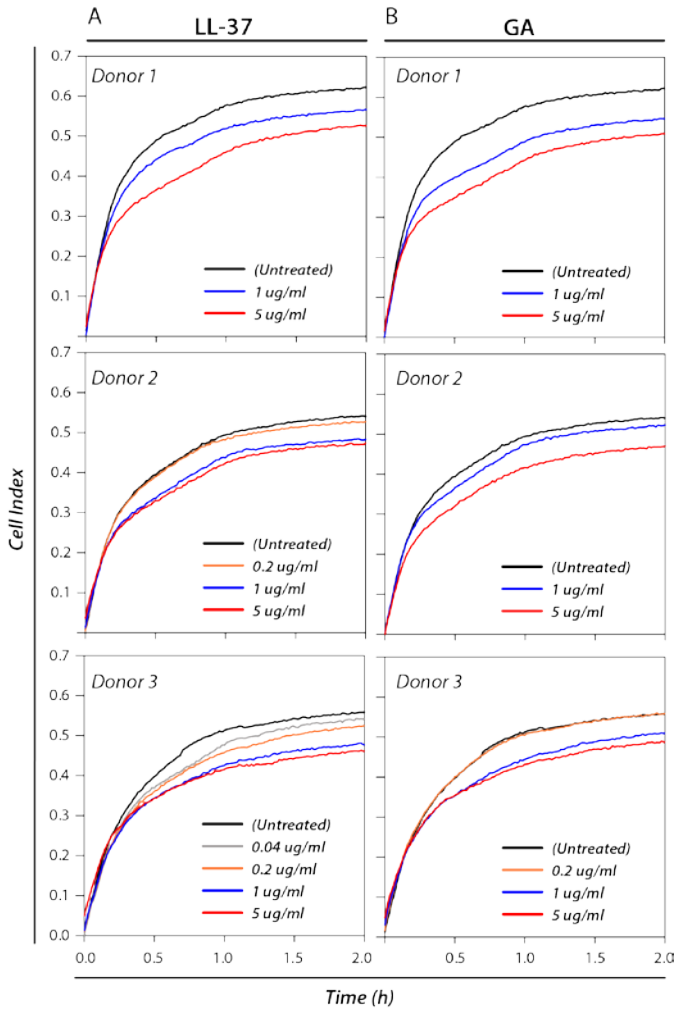

ECIS analysis of the surface contact made by primary T lymphocytes in the presence of 0.04-5 µg/ml of either LL-37 (*A*) or GA (*B*) or absence of these compounds ("no treatment"). Analyses were made with cells from three donors as indicated. Depending on T lymphocytes purification yields experiments were made with a concentration range of cationic compounds from 0.2-5 µg/ml. All experiments included concentrations of 1 and 5 µg/ml and untreated controls ("No treatment").

Lytic properties of GA

The similar effects of GA and LL-37 on leukocytes, notably the quickly induced cell death, raised the question if the lytic properties known for LL-37 (37,38) are shared with GA, notably the ability to lyse simple liposomes.

The GA was applied in two different forms, as dialyzed against isotonic buffer (retentate), or as found in the dialysate , *i.e.*, GA co-polymers sufficiently small for passing through a membrane with a cut-off at 10 kDa. Liposomes were made from 100% 1,2-dioleoyl-sn-glycero-3-phosphocholine (DOPC) to mimic the content of the zwitterionic mammalian cell membranes. Other liposomes, made from 80% DOPC and (the anionic) 20% 1,2-dioleoyl-sn-glycero-3-phospho-rac-(1-glycerol) (DOPG), mimicked the

composition of gram-negative bacteria (25,39). Both types of liposomes were loaded with the dye calcein. The release of dye reached a stable level after 35 min following mixing with GA (data not shown). This level was plotted as a function of GA concentration (Fig. 10A, B).

Fig. 10; Christiansen *et al.*

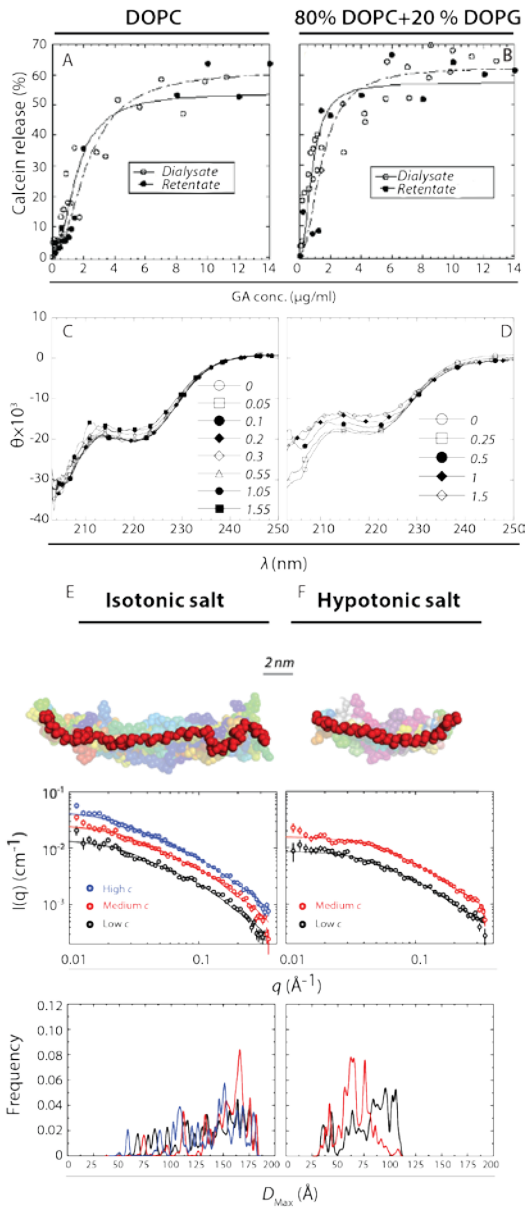

Liposome lysis by GA. *A-B*, Calcein-loaded liposomes made from DOPC (*A*) or 80% or DOPC + 20% DOPG (molar ratio) (*B*) were mixed with the GA in concentrations indicated in the legend. The normalized leakage of calcein (*L*) was determined by fluorimetry and expressed in percent using the formula $L = 100\% \cdot \frac{F - F_0}{F_{Max} - F_0}$ **, where *F* is fluorescence in the presence of GA, F_0 is the reference fluorescence in the absence of GA, and F_{Max} is the maximal fluorescence induced by complete liposomal lysis in the presence of 1% (v/v) Triton X-100. Data were pooled from two independent experiments and fitted to a model for simple cooperative binding, indicated with solid and hatched curves for dialysate and rentate, respectively. *C-D*, Circular dichroism spectroscopy on GA in contact with liposomes made from DOPC (*C*) or DOPC and DOPG (*D*). The molar ellipticity (θ, in deg·cm^2·dmol^{-1}) is plotted as a function of the wavelength (λ). *E-F*, Chemical character of intermolecular interactions by GA co-polymers assessed by SAXS. The molecular envelopes and size distribution of the GA co-polymers were determined at isotonic salt concentration (*E*) and hypotonic salt concentration (*F*). For each analysis, an ensemble of envelopes is shown with the averaged structure indicated in red. Spectra were recorded at either three (*E*) or two concentrations of GA at 1.3, 2.6, or 5.3 mg/ml. Finally, the distributions in D_{Max} for each of these recordings are shown.**

Antimicrobial peptides such as ovispirin, a cationic peptide of the ovine cathelicidin sheep myeloid antimicrobial peptide 29, and the engineered ovispirin-like peptide novicidin (40,41) show a preference for lysing liposome with a gram-negative bacteria-like membrane composition (25). GA showed no such selectivity towards any of the two types of liposomes. To obtain reliable estimates of the plateau for fractional leakage, data were fitted to a simple cooperative fit as shown with curves in the plot. For the GA retentate and the GA dialysate, respectively, these fits (42) yielded plateau levels at 61.4±2.8% and 54.0±3.7% for PC lipids. For PC:PG lipids, these values were 57.5±2.5% and 62.6±4.7%. These values are not significantly different from each other and confirm that GA is not highly sensitive to the lipid charge on the vesicles it disrupts. A roughly similar specific activity per-µg of the raw and dialyzed GA (both retentate and dialysate) suggested that GA's ability to lyse vesicles did not depend on GA size. As expected from these measurements, the raw GA formulation did not behave differently from the dialyzed GA (data not shown). The efficacy of GA, expressed as the number of lipid molecules per GA co-polymer at 50% lysis, corresponds to ~18 lipids per co-polymer.

Co-incubation of GA and liposomes did not significantly alter the secondary structure of the co-polymers according to circular dichroism spectroscopy (Fig. 10C, D). Indeed, the recorded spectra closely resembled those made by us earlier on GA using synchrotron radiation circular dichroism (8). This contrasts with LL-37 (37) or novicidin where liposomes containing DOPG induced major increases in α-helicity (25,40).

To better understand the molecular forces regulating the GA co-polymer interactions and aggregations state, samples with isotonic and hypotonic conditions were investigated by small-

angle X-ray scattering (SAXS). These conditions were obtained by dialysis also removing the high content of mannitol in the clinical formulation, which would otherwise impede the SAXS analysis. Specifically, based on recent findings demonstrating the importance of LL-37 oligomerization through shielding of hydrophobic moieties (37), we determined the oligomeric properties of the co-polymers through three approaches.

First, the model-free IFT analysis showed that the co-polymers in isotonic buffer had a maximum internal distance (D_{Max}) of ~16 nm. By contrast, in the hypotonic buffer the size was reduced to 7 nm. The radius of gyration (R_G) was similar reduced (Table I). The M_r in hypotonic buffer was estimated to ~6,000, not far from the previously reported value at 8,030±170 (6), in particular considering that the two determinations employ different experimental techniques.

Second, a semiflexible polymer model was fitted to the data. The flexibility is described by the Kuhn length (43,44), which was found not to be influenced by the ionic strength of the medium (Table I) and to have a rather high value. The SAXS data could be fitted with a fixed Kuhn length of 30 nm, which suggests a rigid structure of the rods formed by GA. The contour length of the polymer chains was also a fit parameter and the fits showed that the co-polymers were 2-fold longer in isotonic buffer at ~20 nm compared with ~9 nm in the hypotonic buffer in agreement with the results from the IFT analysis. It was particular noteworthy that the chains had a physical length shorter than the Kuhn length (Table I), indicating a large stiffness.

The structural heterogeneity of the random co-polymers was further modelled using the EOM methods (30). The results with regard to their structures from this approach are a set of differently shaped molecules, in isotonic (Fig. 10E) and in hypotonic buffer (Fig. 10F). The results agreed well with the observation made above that the co-polymers, either in their monomeric or dimeric state, formed nearly rigid rods differing mainly in lengths due to an end-end association.

Table I: GA determined structural characterization by IFT analysis or a Gaussian chain polymer model[a]

		IFT Analysis[a]			***Semiflexibles Polymer Model[g]***		
Ionic[b] strength	**GA conc.[c] [mg/ml]**	M_w[d] ± SD **[kDa]**	R_g[e] ± SD **[Å]**	D_{Max}[f] ± SD **[Å]**	L[h] ± SD **[Å]**	R ± SD[¨] **[Å]**	**Kuhn length[j] [Å]**
Hypotonic Buffer	*5.3 mg/ml*	5.4±1	21.0±1	70±10	76 ±12	10 ±0.6	300
	2.6 mg/ml	5.6±1	22.7±1	70±10	79 ±5	9.3 ±0.5	300
	1.3 mg/ml	6.2±1	24.4±1	70±10	108 ±8	8.1 ±0.8	300
Isotonic Buffer	*5.3 mg/ml*	11.1±1	51.0±1	160±10	-	-	-
	2.6 mg/ml	10.0±1	49.7±1	160±10	171 ±11	6.4 ±1.5	300
	1.3 mg/ml	11.1±2	49.5±1	150±10	178 ±16	6.3 ±2.5	300

[a]Values for the GA solution structure estimated by the IFT analysis or a Gaussian chain polymer model. [b,c]Samples with different ionic strengths (hypo or isotonic buffer) or concentration of GA co-polymers were applied in the experiments. [d]Molecular weight, [e]radius of gyration and [f]maximum internal distance (D_{Max}) in the GA copolymers. [g]Parameters from an analytical model describing with Gaussian statistics GA as flexible co-polymers. [h]Length and [i]radius of co-polymers. [j]The Kuhn length, equivalent of two times the persistence length, was calculated as described earlier. Measured values were stated as the mean value±SD. Values for 5.3 mg/ml GA in isotonic buffer were not estimable with polymer model.

Discussion

Although positively-charged AMPs can rapidly disrupt microbial membranes, most positively-charged peptides have generally been considered to be relatively less toxic to eukaryotic cells. Our work now shows that the AMP LL-37 rapidly eliminates certain subsets of leukocytes, probably depending on their presentation of negatively charged carbohydrates in the cell membrane. Surprisingly, these findings also add a novel perspective on the pharmacological mode-of-action of the polymeric formulation GA, a first generation nanomedicine.

In the classic view of cationic peptides, their membrane destabilizing or pore-forming ability is tuned to not damage host tissue while killing membrane-clad microbial organisms. The zwitterionic character of mammalian cell membranes, as well as the cholesterol content, would presumably protect against lysis by cationic peptides while the anionic character of bacterial membranes renders these organisms susceptible (19). However, this dichotomy is not universal among the AMPs. LL-37 has long been known to lyse leukocyte cell lines or erythrocytes (21,45). As addressed below, the random GA co-polymers share cationicity and amphipathicity with LL-37, which enable both compounds to kill primary human leukocytes, even in media with physiologic concentrations of protein and salts. Such killing was achievable within only 30 min of incubation, the shortest time interval permitting reproducible handling in our assays. In principle, the duration of these incubations could be increased. However, with the relatively short half-life of free GA in vivo, it seems reasonable to focus on the consequence of the shorter incubation time as done below.

From several experiments with flow cytometry, it was evident that leukocyte killing of either GA or LL-37 was associated with a considerable formation of vesicles or debris containing remnant proteins from leukocyte cell membranes, *e.g.*, CD45. This phenomenon also permitted imaging of the process of damage. Among the 7AAD-positive, dead cells exposed to GA, those cells carrying a GA-load presented a more irregular cell membrane shape than those without such a

load. Inspection of the images clearly suggested a process involving vesicle formation, with such CD45-positive formations budding from the cell membrane. By contrast, we were not able to detect any induction of Annexin V staining following treatment with GA or LL-37 (data not shown). Taken together with the fast cellular killing by GA, it seems unlikely that the killing involves elaborate cellular processes such as apoptosis. Indeed, induction of apoptosis in model systems was reported to require 12-18 h of incubation with strong agents such as ionomycin or staurosporine (46). A more likely explanation, also consistent with the marked formation of debris, involves a direct damage to the cell membrane. The cell membrane fragmentation enabled the use of more sensitive methodologies to follow the impact of GA and LL-37 treatment. Simple forward scatter measurements clearly indicated that LL-37 was capable of producing debris of subcellular sizes, while this did not happen when GA was used, even in high concentration. Using the more advanced NTA particle tracking technology, we demonstrated that GA produced debris with sizes between 180-500 nm, while these smaller particles were not robustly generated by LL-37. This enabled furthermore detection of the cell fragmentation down to a concentration of 1 µg/ml GA, tightly reproduced among the donors tested. Particularly in the NTA experiments, it was evident that untreated leukocytes produce particulate material in a size-range similar to those particles released when the cells were treated with GA. It is known, of course, that T and B lymphocytes are producers of exosomes, vesicles with sizes of 60-100 nm (47). While we cannot conclude that exosomes are not a part of the material generated by GA and LL-37 treatment, we believe the full picture of the events must also include the experiments made with flow cytometry. In the latter type of experiment, the increase in low-forward scatter material came with an increase in 7AAD staining, *i.e.*, cell death. With this observation, it seems more likely that the fragments formed by GA and LL-37 treatment are debris rather than necessarily similar to exosomes formed by living cells.

In determining what concentrations are therapeutically relevant, it is noteworthy that the pharmacokinetics of GA is not well established (7,48). Beyond the conditions at the site of injection, reports also suggest that partially hydrolyzed co-polymers may reach regional lymph nodes while there is a scarcity of evidence for the presence in other secondary lymphoid tissue such as the spleen (7,48). Considering the vast body of evidence supporting long-term influences on the immune system and GA antigenic properties (3), there seems to be little doubt that the presence in lymphoid tissues (48) may play a role in modulating the adaptive immune response and produce some of the therapeutic effects of GA. However, with the recent observation that GA also modulates the immune system in short time intervals (49), mechanisms with such an ability are obviously of interest. The skin, *i.e.*, the site of injection, is a fully immunocompetent region of the body, including a large presence of several types of T lymphocytes (50). Following therapeutic administration of 36 mg GA into this environment, the relevant local concentration may easily exceed the concentrations used in our study. The activity of most peptidic antimicrobials is sensitive to the chemical environment, in particular with regard to salt concentration and protein content. The subcutaneous environment could, at least in principle, expose GA to interstitial fluids, lymph, or plasma. Although progress has been made in the proteomic characterization of lymph, it is clear that this fluid contain variable constituents, depending on, for instance, site of collection (51). We tested GA in buffer with 40 mg/ml HSA, *i.e.*, close to the concentration in human plasma, and with the divalent metal ions Ca^{2+} and Mg^{2+}. Albeit these additions may not precisely mimic the more complex body fluids, the high protein content and metal ions are pertinent parts of these fluids (23,51). In such buffer, GA maintained detectable cytolytic activity at 25 µg/ml, suggesting that GA may kill leukocytes in the subcutaneous environment.

Measurements on the contact between T lymphocytes using electrical impedance also recorded effects at modest concentrations. Impedance sensing for probing morphological changes in

cell-substrate contact was initially developed to monitor changes on the nm-scale non-invasively (52). Considering the sizes of the debris determined by NTA, it seems reasonable to propose that the ECIS recordings reflect the same process of debris formation as observed in our other experiments. Similar to the observations made with NTA, a concentration of ~1 µg/ml LL-37 or GA was sufficient to alter the response. This agrees with other studies showing that ECIS can detect cell death through the concomitant change in contact with the substrate (53). In our study, a plateau in the cell index value was quickly reached. When the cell index was compared between untreated and treated samples, it was clear that treatment reduced the plateau response, which remained stable for hours. This is consistent with a rapid killing by LL-37 and GA of a select group of the T lymphocytes applied in the experiment as observed in the flow cytometry experiments.

By use of engineered LUVs, we found that GA is able to lyse both negatively charged and zwitterionic liposomes with similar specific activity, a property not shared with naturally occurring cathelidicins (39,54). However, compared with the activity of other engineered anti-microbial peptides such as novicidin (25), GA is only moderately effective and on a per-mg basis approximately 10-fold less active than α-synuclein, which is a confirmed cytolytic protein (55). However, in our experiments the tested LUVs did not carry HS or sialic acid characteristic of the mammalian cell membrane. Our study and the report by Koenig *et al.* (12) suggest that such charged carbohydrates are critical for efficient GA binding and cell killing. The studies using circular dichroism spectroscopy also pointed to differences between GA and other membrane disrupting peptides, notably LL-37 and novicidin. Unlike these peptides, GA does not alter secondary structure content. As one explanation, this would originate through a looser contact between GA and the target membrane compared with LL-37 and ovispirin.

Several studies have now clearly demonstrated the ability of LL-37 to form oligomers with a loose hydrophobic core under physiological conditions (37,56,57). Apparently, this

oligomerization, or the character of peptides able to form such structures, is critical to the function of peptides of the LL-37 group, more so than specific size, sequence, or charge distribution (56). Indeed, the ability of both GA and LL-37 to lyse human cells with almost equal specific activity is a strong support of Zelezetsky *et al.*'s observation that no single primary structure is a determinant in the cytolytic functions of LL-37-like peptides (56). Recently, from dynamic light scattering studies of GA, the formation of larger oligomers were reported, although the chemical principles making such oligomerization were not investigated (9). It should be noted that in this study the intensity-weighted GA size distributions from dynamic light scattering were reported with the observation of a large component around 100 nm (9). This was interpreted as the presence of colloidal nanoparticles. Importantly, conversion done by us into a volume distribution showed that only ~1% of the sample is in this form of nanoparticles, while the rest are molecularly disperse polypeptides with an average hydrodynamic size of about 5-7 nm. We now show by SAXS analysis that GA copolymers, like LL-37, also form small oligomers (dimers), in isotonic buffer, but clearly with a possibility that larger oligomers can be formed as well under other conditions. These oligomers are kept together by shielding of the hydrophobic side chains as judged from their dissolution in hypotonic buffer. As noted from the comparison with LL-37, this propensity to oligomerize is likely to be critical for the cell lysis activity and, at the same time, explains why GA may form small nanoparticles. In this way, the oligomerization supports GA as part of first-generation nanomedicine (9,10).

Conclusions

Our report now points to previously unappreciated effects of GA on human leukocytes, notably its ability to rapidly kill mainly subsets of T lymphocytes. From a mechanistic view point, the GA cell killing involves sialic acid. From the above experiment, we propose a model, which permit a weak

interaction with the anionic cell membrane. Full disruption of the cellular membrane requires further support from interaction with the sialylated proteins in the membrane (Fig. 11). This mechanism is shared with LL-37. LL-37 and other cathelicidins are evolutionary conserved AMPs, but they also carry profound influences directly on the host immune system. For this reason, it encourages the suggestion that the pharmacology of GA, at least in part, involves the use of an ancient regulatory mechanism of the innate immune system, which depend on cationic co-polymers forming oligomers with a loose hydrophobic core. This notion is already supported in the literature where the fast onset of the immunomodulatory effects of GA in treated patients (49) agrees well with the short time scale for action also observed in our study. Furthermore, it is well established in the treatment of MS patients that T lymphocytes are an important target as highlighted by the recent application of alemtuzumab. This antibody binds the T lymphocyte antigen CD52 and precipitates a rapid depletion of circulating lymphocytes, probably through antibody-dependent cell-mediated cytotoxicity (58). While this treatment may appear as a more powerful tool to dampen inflammation, it also contains the risk of adverse side effects such as infections. The remarkable safety of GA treatment and its well-documented effects in MS treatment heightens the interest in this formulation and other similar polymers devised for immunotherapy (2). The link between GA as a nanomedicine and its lysis of leukocytes is likely to aid the improved design of a class of polymers with such immunomodulatory effects.

Fig. 11; Christiansen *et al.*

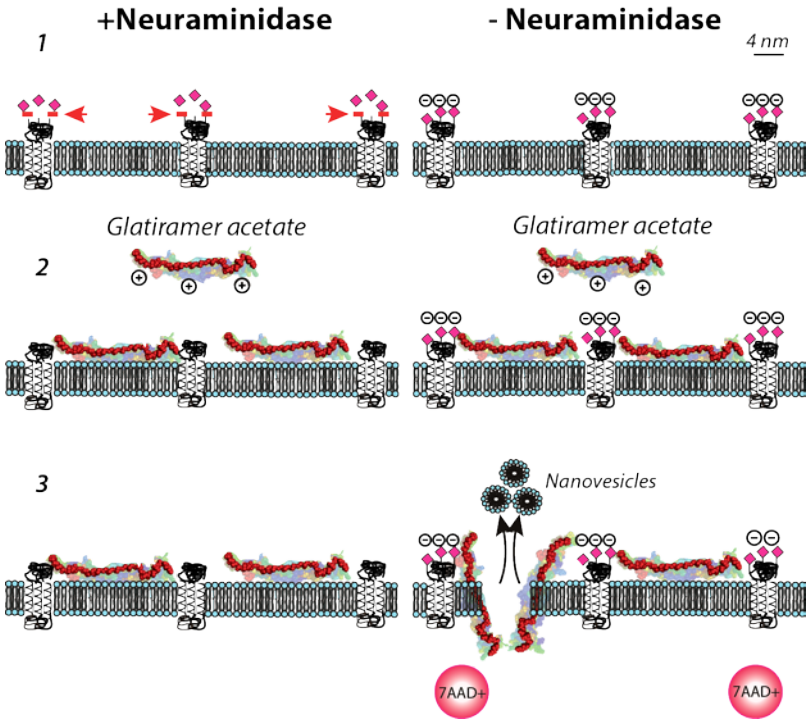

The graphical abstract depicts two scenarios; (1) an untreated cell membrane and a cell membrane treated with neuraminidase to remove cell-surface sialic acids from glycoproteins embedded in the plasma membrane (cutting indicated with arrowheads). Both the neuraminidase-treated and untreated cell membrane are rich in negatively charged phospholipids. Sialic acid provide a large component of negative charge to the cell membrane in the untreated cells. Hence, (2) the removal of cell surface sialic acids alters the interaction between the positively-charged GA copolymer and the cell membrane. In both scenarios, GA binds the cell membrane loosely with no major insertion, as judged from the circular dichroism experiments described in our paper. (3) The expression of sialic acid on the membrane enhances the electrostatic interaction between the GA copolymers and the cell membrane. This increased electrostatic interaction enable the GA copolymers to effectively attach and insert themselves into membrane bilayers, which ultimately results in a 7AAD+ nonviable cell and formation of nanovesicles. The figure is drawn to approximate scale using the SAXS-modeled GA dimer.

Acknowledgements

The work was generously supported by grants from the Danish Multiple Sclerosis Association (R192-A10117-B143, R266-A14659-B143 & R308-A19315-B143) and The Novo Nordisk Foundation (R179-A15255). Our project was carried out in the context of The Lundbeck Foundation Nanomedicine Center for Individualized Management of Tissue Damage and Regeneration as well as the Center for Neurodegenerative Inflammation Prevention and MEMBRANES Research Center supported by the Aarhus University Research Foundation. We thank Professor Finn Sellebjerg, Rigshospitalet, University of Copenhagen, and Dr. Thor Petersen, Aarhus University Hospital for inspiration. We thank Professor Bent W. Deleuran and Dr. Halldór Bjarki Einarsson, Aarhus University Hospital, for helpful comments and Bettina W. Grumsen for excellent technical assistance in designing and executing the experiments. The FACS Core Facility within Dept. of Biomedicine, Aarhus University, is kindly acknowledged for their help in analyzing data

References

1. Duncan, R. (2014) Polymer therapeutics: Top 10 selling pharmaceuticals - what next? *J Control Release* **190**, 371-380
2. Jalilian, B., Einarsson, H. B., and Vorup-Jensen, T. (2012) Glatiramer Acetate in Treatment of Multiple Sclerosis: A Toolbox of Random Co-Polymers for Targeting Inflammatory Mechanisms of both the Innate and Adaptive Immune System? *Int J Mol Sci* **13**, 14579-14605
3. Sela, M., and Mozes, E. (2004) Therapeutic vaccines in autoimmunity. *Proc Natl Acad Sci U S A* **101 Suppl 2**, 14586-14592
4. Arnon, R., and Sela, M. (2003) Immunomodulation by the copolymer glatiramer acetate. *J Mol Recognit* **16**, 412-421
5. Chen, C. (2016) Immunomodulation of Glatiramer Acetate in Multiple Sclerosis. *Neurochem Neuropharm* **2**, 1
6. Rogstad, S., Pang, E., Sommers, C., Hu, M., Jiang, X., Keire, D. A., and Boyne, M. T., 2nd. (2015) Modern analytics for synthetically derived complex drug substances: NMR, AFFF-MALS, and MS tests for glatiramer acetate. *Anal Bioanal Chem* **407**, 8647-8659
7. Varkony, H., Weinstein, V., Klinger, E., Sterling, J., Cooperman, H., Komlosh, T., Ladkani, D., and Schwartz, R. (2009) The glatiramoid class of immunomodulator drugs. *Expert Opin Pharmacother* **10**, 657-668
8. Stapulionis, R., Oliveira, C. L., Gjelstrup, M. C., Pedersen, J. S., Hokland, M. E., Hoffmann, S. V., Poulsen, K., Jacobsen, C., and Vorup-Jensen, T. (2008) Structural insight into the function of myelin basic protein as a ligand for integrin alpha M beta 2. *J Immunol* **180**, 3946-3956
9. Conner, J. B., Bawa, R., Nicholas, J. M., and Weinstein, V. (2014) Copaxone® in the era of biosimilars and nanosimilars. in *Handbook of Clinical Nanomedicine - From Bench to Bedside* (Bawa, R., Audette, G. F., and Rubinstein, I. eds.), Pan Stanford Publishing Pte Ltd, Singapore
10. Duncan, R., and Gaspar, R. (2011) Nanomedicine(s) under the microscope. *Mol Pharm* **8**, 2101-2141
11. Brenner, T., Arnon, R., Sela, M., Abramsky, O., Meiner, Z., Riven-Kreitman, R., Tarcik, N., and Teitelbaum, D. (2001) Humoral and cellular immune responses to Copolymer 1 in multiple sclerosis patients treated with Copaxone. *J Neuroimmunol* **115**, 152-160
12. Koenig, P. A., Spooner, E., Kawamoto, N., Strominger, J. L., and Ploegh, H. L. (2013) Amino acid copolymers that alleviate experimental autoimmune encephalomyelitis in vivo interact with heparan sulfates and glycoprotein 96 in APCs. *J Immunol* **191**, 208-216
13. Teitelbaum, D., Meshorer, A., Hirshfeld, T., Arnon, R., and Sela, M. (1971) Suppression of experimental allergic encephalomyelitis by a synthetic polypeptide. *Eur J Immunol* **1**, 242-248
14. Chelmicka-Szorc, E., and Arnason, B. G. (1975) Suppression of experimental allergic encephalomyelitis in guinea-pigs with poly-L-lysine. *Clin Exp Immunol* **22**, 539-545
15. Kahlenberg, J. M., and Kaplan, M. J. (2013) Little peptide, big effects: the role of LL-37 in inflammation and autoimmune disease. *J Immunol* **191**, 4895-4901
16. Wang, G. S., Mishra, B., Epand, R. F., and Epand, R. M. (2014) High-quality 3D structures shine light on antibacterial, anti-biofilm and antiviral activities of human cathelicidin LL-37 and its fragments. *Biochimica Et Biophysica Acta-Biomembranes* **1838**, 2160-2172

17. Frasca, L., and Lande, R. (2012) Role of defensins and cathelicidin LL37 in auto-immune and auto-inflammatory diseases. *Curr Pharm Biotechnol* **13**, 1882-1897

18. Hilchie, A. L., Wuerth, K., and Hancock, R. E. (2013) Immune modulation by multifaceted cationic host defense (antimicrobial) peptides. *Nat Chem Biol* **9**, 761-768

19. Brogden, K. A. (2005) Antimicrobial peptides: pore formers or metabolic inhibitors in bacteria? *Nat Rev Microbiol* **3**, 238-250

20. Ong, P. Y., Ohtake, T., Brandt, C., Strickland, I., Boguniewicz, M., Ganz, T., Gallo, R. L., and Leung, D. Y. (2002) Endogenous antimicrobial peptides and skin infections in atopic dermatitis. *N Engl J Med* **347**, 1151-1160

21. Johansson, J., Gudmundsson, G. H., Rottenberg, M. E., Berndt, K. D., and Agerberth, B. (1998) Conformation-dependent antibacterial activity of the naturally occurring human peptide LL-37. *J Biol Chem* **273**, 3718-3724

22. Bandholtz, L., Ekman, G. J., Vilhelmsson, M., Buentke, E., Agerberth, B., Scheynius, A., and Gudmundsson, G. H. (2006) Antimicrobial peptide LL-37 internalized by immature human dendritic cells alters their phenotype. *Scand J Immunol* **63**, 410-419

23. Kragh-Hansen, U., Minchiotti, L., Galliano, M., and Peters, T., Jr. (2013) Human serum albumin isoforms: genetic and molecular aspects and functional consequences. *Biochim Biophys Acta* **1830**, 5405-5417

24. Millipore, A.-p. o. E. (2015) IDEAS® Image Data Exploration and Analysis Software User's Manual. https://www.amnis.com/images/PN_780-00959-00_RevC_IDEAS_User_Manual.pdf

25. Balakrishnan, V. S., Vad, B. S., and Otzen, D. E. (2013) Novicidin's membrane permeabilizing activity is driven by membrane partitioning but not by helicity: a biophysical study of the impact of lipid charge and cholesterol. *Biochim Biophys Acta* **1834**, 996-1002

26. Pedersen, J. S. (2004) A flux- and background-optimized version of the NanoSTAR small-angle X-ray scattering camera for solution scattering. *J. Appl. Crystallography* **37**, 369-380

27. Glatter, O. (1977) New method for evaluation of small-angle scattering data. *J. Appl. Cryst* **10**, 415-421

28. Pedersen, J. S., Hansen, S., and Bauer, R. (1994) The aggregation behavior of zinc-free insulin studied by small-angle neutron scattering. *Eur Biophys J* **22**, 379-389

29. Pedersen, J. S., and Schurtenberger, P. (1996) Scattering Functions of Semiflexible Polymers with and without Excluded Volume Effects. *Macromolecules* **29**, 7602-7612

30. Bernado, P., Mylonas, E., Petoukhov, M. V., Blackledge, M., and Svergun, D. I. (2007) Structural characterization of flexible proteins using small-angle X-ray scattering. *J Am Chem Soc* **129**, 5656-5664

31. Mader, J. S., Mookherjee, N., Hancock, R. E., and Bleackley, R. C. (2009) The human host defense peptide LL-37 induces apoptosis in a calpain- and apoptosis-inducing factor-dependent manner involving Bax activity. *Mol Cancer Res* **7**, 689-702

32. Mader, J. S., Marcet-Palacios, M., Hancock, R. E., and Bleackley, R. C. (2011) The human cathelicidin, LL-37, induces granzyme-mediated apoptosis in cytotoxic T lymphocytes. *Exp Cell Res* **317**, 531-538

33. Bjorstad, A., Askarieh, G., Brown, K. L., Christenson, K., Forsman, H., Onnheim, K., Li, H. N., Teneberg, S., Maier, O., Hoekstra, D., Dahlgren, C., Davidson, D. J., and Bylund, J. (2009) The host defense peptide LL-37 selectively permeabilizes apoptotic leukocytes. *Antimicrob Agents Chemother* **53**, 1027-1038

34. Zhang, Z., Cherryholmes, G., and Shively, J. E. (2008) Neutrophil secondary necrosis is induced by LL-37 derived from cathelicidin. *J Leukoc Biol* **84**, 780-788

35. Durr, U. H., Sudheendra, U. S., and Ramamoorthy, A. (2006) LL-37, the only human member of the cathelicidin family of antimicrobial peptides. *Biochim Biophys Acta* **1758**, 1408-1425

36. Jones, K. S., Petrow-Sadowski, C., Bertolette, D. C., Huang, Y., and Ruscetti, F. W. (2005) Heparan sulfate proteoglycans mediate attachment and entry of human T-cell leukemia virus type 1 virions into CD4+ T cells. *J Virol* **79**, 12692-12702

37. Xhindoli, D., Pacor, S., Guida, F., Antcheva, N., and Tossi, A. (2014) Native oligomerization determines the mode of action and biological activities of human cathelicidin LL-37. *Biochem J* **457**, 263-275

38. Zhao, C., Nguyen, T., Boo, L. M., Hong, T., Espiritu, C., Orlov, D., Wang, W., Waring, A., and Lehrer, R. I. (2001) RL-37, an alpha-helical antimicrobial peptide of the rhesus monkey. *Antimicrob Agents Chemother* **45**, 2695-2702

39. Schmidt, N. W., and Wong, G. C. (2013) Antimicrobial peptides and induced membrane curvature: Geometry, coordination chemistry, and molecular engineering. *Current Opin Solid State Mater Science* **17**, 151-163

40. Dorosz, J., Gofman, Y., Kolusheva, S., Otzen, D., Ben-Tal, N., Nielsen, N. C., and Jelinek, R. (2010) Membrane interactions of novicidin, a novel antimicrobial peptide: phosphatidylglycerol promotes bilayer insertion. *J Phys Chem B* **114**, 11053-11060

41. Khandelia, H., and Kaznessis, Y. N. (2006) Molecular dynamics investigation of the influence of anionic and zwitterionic interfaces on antimicrobial peptides' structure: implications for peptide toxicity and activity. *Peptides* **27**, 1192-1200

42. Wimmer, R., Andersen, K. K., Vad, B., Davidsen, M., Molgaard, S., Nesgaard, L. W., Kristensen, H. H., and Otzen, D. E. (2006) Versatile interactions of the antimicrobial peptide novispirin with detergents and lipids. *Biochemistry* **45**, 481-497

43. Kuhn, W. (1934) Concerning the shape of thread shapes molecules in solution. *Kolloid-Zeitschrift* **68**, 2-15

44. Kratky, O., and Porod, G. (1949) Rontgenuntersuchung Geloster Fadenmolekule. *J Royal Netherlands Chem Soc* **68**, 1106-1122

45. Thennarasu, S., Tan, A., Penumatchu, R., Shelburne, C. E., Heyl, D. L., and Ramamoorthy, A. (2010) Antimicrobial and membrane disrupting activities of a peptide derived from the human cathelicidin antimicrobial peptide LL37. *Biophys J* **98**, 248-257

46. Devitt, A., and Gregory, C. D. (2004) Measurement of apoptotic cell clearance in vitro. *Methods Mol Biol* **282**, 207-221

47. Dustin, M. L. (2014) What counts in the immunological synapse? *Mol Cell* **54**, 255-262

48. McKeage, K. (2015) Glatiramer Acetate 40 mg/mL in Relapsing-Remitting Multiple Sclerosis: A Review. *CNS Drugs* **29**, 425-432

49. Ayers, C. L., Mendoza, J. P., Sinha, S., Cunnusamy, K., Greenberg, B. M., Frohman, E. M., and Karandikar, N. J. (2013) Modulation of immune function occurs within hours of therapy initiation for multiple sclerosis. *Clin Immunol* **147**, 105-119

50. Fan, X., and Rudensky, A. Y. (2016) Hallmarks of Tissue-Resident Lymphocytes. *Cell* **164**, 1198-1211

51. Hansen, K. C., D'Alessandro, A., Clement, C. C., and Santambrogio, L. (2015) Lymph formation, composition and circulation: a proteomics perspective. *Int Immunol* **27**, 219-227

52. Giaever, I., and Keese, C. R. (1993) A morphological biosensor for mammalian cells. *Nature* **366**, 591-592

53. Opp, D., Wafula, B., Lim, J., Huang, E., Lo, J. C., and Lo, C. M. (2009) Use of electric cell-substrate impedance sensing to assess in vitro cytotoxicity. *Biosens Bioelectron* **24**, 2625-2629

54. Yeaman, M. R., and Yount, N. Y. (2003) Mechanisms of antimicrobial peptide action and resistance. *Pharmacol Rev* **55**, 27-55

55. van Rooijen, B. D., Claessens, M. M., and Subramaniam, V. (2010) Membrane Permeabilization by Oligomeric alpha-Synuclein: In Search of the Mechanism. *PLoS One* **5**, e14292

56. Zelezetsky, I., Pontillo, A., Puzzi, L., Antcheva, N., Segat, L., Pacor, S., Crovella, S., and Tossi, A. (2006) Evolution of the primate cathelicidin. Correlation between structural variations and antimicrobial activity. *J Biol Chem* **281**, 19861-19871

57. Xhindoli, D., Morgera, F., Zinth, U., Rizzo, R., Pacor, S., and Tossi, A. (2015) New aspects of the structure and mode of action of the human cathelicidin LL-37 revealed by the intrinsic probe p-cyanophenylalanine. *Biochem J* **465**, 443-457

58. Willis, M. D., and Robertson, N. P. (2016) Alemtuzumab for Multiple Sclerosis. *Curr Neurol Neurosci Rep* **16**, 84